Increased nonHDL cholesterol levels cause muscle wasting and ambulatory dysfunction in the mouse model of LGMD2B[S]

Stephanie L. Sellers,[1,*,†] Nadia Milad,[1,*,†] Zoe White,[*,†] Chris Pascoe,[†,§] Rayleigh Chan,[*,†] Geoffrey W. Payne,[***] Chun Seow,[*,†] Fabio Rossi,[§,,††] Michael A. Seidman,[†,§§] and Pascal Bernatchez[2,*,†]**

Department of Anesthesiology, Pharmacology & Therapeutics and UBC Centre for Heart Lung Innovation,* St. Paul's Hospital,[†] Department of Pathology and Laboratory Medicine,[§] Biomedical Research Centre,** Department of Medical Genetics,[††] University of British Columbia, Vancouver, Canada; and Department of Pathology,[§§] Providence Health Care, University of Northern British Columbia,*** Prince George, Canada

Abstract **Progressive limb and girdle muscle atrophy leading to loss of ambulation is a hallmark of dysferlinopathies, which include limb-girdle muscular dystrophy type 2B and Miyoshi myopathy. However, animal models fail to fully reproduce the disease severity observed in humans, with dysferlin-null (Dysf$^{-/-}$) mice exhibiting minor muscle damage and weakness without dramatic ambulatory dysfunction. As we have previously reported significant Dysf expression in blood vessels, we investigated the role of vascular function in development of muscle pathology by generating a Dysf-deficient mouse model with vascular disease. This was achieved by crossing Dysf$^{-/-}$ mice with ApoE$^{-/-}$ mice, which have high levels of nonHDL-associated cholesterol. Double-knockout Dysf$^{-/-}$ApoE$^{-/-}$ mice exhibited severe ambulatory dysfunction by 11 months of age. In limb-girdle muscles, histology confirmed dramatic muscle wasting, fibrofatty replacement, and myofiber damage in Dysf$^{-/-}$ApoE$^{-/-}$ mice without affecting the ratio of centrally nucleated myofibers. Although there were no major changes in ex vivo diaphragm and soleus muscle function, histological analyses revealed these muscles to be untouched by damage and remodelling.[JLR] In all, these data suggest that cholesterol may be deleterious to dysferlinopathic muscle and lead to ambulatory dysfunction. Moreover, differences in plasma lipid handling between mice and humans could be a key factor affecting dysferlinopathy severity.**—Sellers, S. L., N. Milad, Z. White, C. Pascoe, R. Chan, G. W. Payne, C. Seow, F. Rossi, M. A. Seidman, and P. Bernatchez. **Increased non-HDL cholesterol levels cause muscle wasting and ambulatory dysfunction in the mouse model of LGMD2B.** ***J. Lipid Res.*** **2018.** 59: **261–272.**

Supplementary key words dysferlin • muscular dystrophy • atherosclerosis • apolipoproteins • muscle • HDL • animal models

Dysferlinopathies represent a class of inherited muscle disorders caused by mutations in the dysferlin (Dysf) gene (1). These include limb-girdle muscular dystrophy (MD) type 2B (LGMD2B), Miyoshi myopathy, and distal anterior compartment myopathy, which all lead to progressive muscle wasting of limb and girdle muscles with significant or complete loss of ambulatory function (2). Mechanistic evidence suggests that loss of normal Dysf expression results in insufficient repair of the plasma membrane due to blunted lipid patch fusion and abnormal trafficking of transmembrane proteins (1, 3). This patch-dependent system of membrane repair is important in tissues undergoing constant stress and injury such as skeletal muscle myofibers (4), where loss of expression leads to progressive muscle degeneration and inflammation, all of which are observed in LGMD2B and Myoshi myopathy patients (5–7). However, there are still no effective and approved pharmacological treatments for dysferlinopathies. Compared with human LGMD2B, mouse models of dysferlinopathies exhibit only minor myofiber wasting observable on skeletal muscle histology and, although ambulatory function slowly declines, complete loss of walking ability is rarely observed (1, 8).

Although reconstitution of Dysf expression specifically in skeletal muscle has led to improved muscle function and pathology (8), reports of Dysf expression in nonskeletal muscle tissues, such as cardiac myocytes and inflammatory cells, paint a more complex picture of the disease (9).

This work was supported by grants from the Canadian Institutes of Health Research (CIHR), Heart & Stroke Foundation of Canada and the Jain Foundation to P.B. S.L.S. was supported by a CIHR doctoral fellowship, CIHR Michael Smith Foreign Study Supplement and fellowships from the University of British Columbia.

Manuscript received 28 July 2017 and in revised form 19 October 2017.

Published, JLR Papers in Press, November 25, 2017
DOI https://doi.org/10.1194/jlr.M079459

Abbreviations: CNF, centrally nucleated fiber; Dysf, dysferlin; HDLc, HDL-associated cholesterol; LGMD2B, limb-girdle muscular dystrophy 2B; MD, muscular dystrophy; rec. fem., rectus femoris; TG, triglyceride.

[1] S. L. Sellers and N. Milad contributed equally to this work.

[2] To whom correspondence should be addressed.
e-mail: pascal.bernatchez@ubc.ca

[S] The online version of this article (available at http://www.jlr.org) contains a supplement.

Previous research by our group has shown that loss of Dysf expression causes severe vascular abnormalities such as impaired angiogenesis and endothelial dysfunction (3). This was shown to be the consequence of robust Dysf expression in vascular cells such as smooth muscle and especially endothelial cells. Notably, a two-hit vascular hypothesis was proposed to explain the severity of muscle wasting in other forms of MD, postulating that observed muscle damage arises from areas of anoxia and ischemia caused by blood vessel abnormalities (10, 11). Because evidence of ischemia was not found in MD patients or animal models, most assume that the numerous vascular abnormalities reported are a compensatory response rather than acting as primary contributors to muscle wasting and degeneration (11).

Although evidence of vascular dysfunction in Dysf-deficient MD patients is limited, lipid analysis in LGMD2B muscle revealed a significant increase in triglyceride (TG) levels and decrease in linoleic acid levels compared with unaffected controls (12). As others have reported abnormal plasma and muscle lipid metabolism in other forms of MD and elevated cholesterol levels correlated with muscle pathology severity in some MD patients (13–15), we challenged the dynamic interplay between blood vessels and MD muscle tissues by generating dysferlinopathic mice with elevated levels of "bad,"non HDL-associated cholesterol (HDL*c*) (i.e., VLDL, LDL, and IDL) known to accelerate vascular disease and atherosclerosis by inactivating their ApoE gene (16). To our surprise, $Dysf^{-/-}ApoE^{-/-}$ mice show a significant reduction in stride length followed by complete loss of ambulatory function when on a Western high-fat, high-cholesterol diet, in stark contrast to the notoriously mild phenotype of $Dysf^{-/-}$ mice (1). Histological analyses revealed that loss of ApoE causes dramatic exacerbation of muscle wasting while ex vivo muscle function revealed no major changes in fatigability and force recovery. Our data suggest that heightened levels of nonHDLc could result in complete loss of walking ability in $Dysf^{-/-}$ mice, leading to a more representative model of LGMD2B. This study also calls for further investigation of plasma cholesterol-related abnormalities in dysferlinopathies as a primary contributor to muscle damage exacerbation, fibrofatty replacement, and ambulation dysfunction rather than a consequence of myofiber degeneration or an unrelated coincidence.

MATERIALS AND METHODS

Animals

All use of animals was approved by the Animal Care and Use Committee at the University of British Columbia. All animals were housed in the Genetically Engineered Models Facility at the Centre for Heart Lung Innovation on a 12 h light/dark cycle and given access to food and water ad libitum. Colony founding $Dysf^{-/-}$ mice were obtained from the Jackson Laboratory ($B6.129Dysf^{tm1Kcam/J}$, stock #013149) and backcrossed onto a C57BL/6 background for greater than 10 generations. Disruption of the Dysf gene was confirmed in $Dysf^{-/-}$ mice via the original PCR protocol developed by and obtained directly from the Campbell laboratory (University of Iowa) using a long range PCR enzyme (Takara, catalog #RR0002M). $ApoE^{-/-}$ mice were obtained from the Jackson Laboratory ($B6.129P2\text{-}Apoe^{tm1Unc/J}$, stock #002052) and disruption of the ApoE gene was confirmed via PCR protocol suggested by the Jackson Laboratory. Generation of experimental $Dysf^{-/-}ApoE^{-/-}$ mice and control groups was achieved by breeding $Dysf^{-/-}$ mice to $ApoE^{-/-}$ to generate $Dysf^{+/-}ApoE^{+/-}$ littermates. These littermates were subsequently bred together to produce $Dysf^{-/-}ApoE^{-/-}$, $Dysf^{-/-}$, $ApoE^{-/-}$, and WT mice. Mice were weaned at 3–4 weeks of age and fed standard laboratory chow containing 6% fat by weight or 13% kcal from fat with no added cholesterol (LabDiet 5001) or with added lipids and cholesterol (Harlan Teklad TD88137 containing 21% fat by weight or 42% kcal from fat with 0.15% added cholesterol) starting at 8 weeks of age.

Gait analysis and gross muscle wasting

Analysis of gait was completed from ink imprint of hind paws recorded on paper from mice walking a five-foot distance. Stride length was defined as the distance between two consecutive imprints from the same foot. Areas in which a mouse paused were not included and overall stride length per mouse was averaged from three replicates. The presence of grossly observable muscle wasting in the hindlimbs was studied from photographs of posteuthanasia animals upon removal of the epidermis, where width was defined as the distance of a line perpendicular to the tibia and measured from the anterior aspect of the tibia to the most posterior point of the gastrocnemius.

Histological analysis

Histological analysis was performed on isolated muscles and hearts fixed for at least 24 h in 10% buffered formalin. Muscles and hearts were subsequently bisected and embedded in paraffin. Analysis was performed on H&E- and Masson's trichrome-stained slides. Total muscle area, myofiber content, and fat accumulation calculations were performed using manual tracing, while fibrosis was measured via positive pixel count using ImageScope software following scanning of Masson's trichrome-stained slides on a high resolution Aperio Scanner. Centrally nucleated fibers (CNFs) were assessed on four randomly selected fields of view. Histological cholesterol pits were assessed as present or absent in multiple consecutive histological sections per animal. Accumulation of inflammatory cells was measured via manual tracing. All histological assessment was performed in a manner blind to genotype and in consultation with a pathologist.

Contralateral muscles were embedded in cross-section in tragacanth, flash frozen in liquid nitrogen-cooled isopentane, and stored at −80°C. Frozen muscles were sectioned at −20°C at 8 μm thickness. Cryosections were stained with Oil Red O to visualized neutral lipids in muscle tissue following the protocol developed by Mehlem et al. (17). To further characterize fatty infiltration, sections were stained for perilipin-1 (Cell Signaling, D1D8 #9349), an adipocyte marker, via immunofluorescence, following the protocol suggested by the manufacturer.

Plasma analysis

Whole blood was collected in heparinized tubes via cardiac puncture of unfasted mice at euthanasia, centrifuged at 3,000 RPM for 10 min at 4°C and plasma stored at −80°C. Plasma samples were assessed using the Siemans Advia 1800 system for levels of cholesterol (CHOL-2), high density lipoprotein (D-HDL) and triglycerides (TRIG-2). Assays were performed following manufacturer's instructions.

Ex vivo muscle myography

Briefly, muscles were isolated and mounted to terminal tendons to a force transducer and stretched to physiological length

in an organ bath of warmed Krebs solution perfused with carbogen (30% oxygen, 70% carbon dioxide). Fatigue was measured over 35 consecutive stimulations and postfatigue recovery assessed as a fraction of the prefatigue force over eight stimulations separated by 30 s intervals.

Echocardiography

Echocardiograms were performed on mice anesthetized with isoflurane using a VisualSonics Vevo 2100 system with a MS-550D 40MHz probe. Body temperature was measured and maintained via a heated platform. Heart rate, breathing rate, and an electrocardiography trace were acquired and monitored by sensors built into the Vevo 2100 imaging platform. All echocardiograms were performed and analyzed by a technician trained in murine echocardiography. A four-chamber view echocardiogram method was utilized to allow left ventricle tracing to determine ventricle size and volume as well as cardiac parameters of cardiac output, ejection fraction, stroke volume, and factional shortening.

Statistical analysis

Statistical analyses were performed using GraphPad Prism 6. For comparison of multiple groups at one time-point, a one-way ANOVA multiple comparison test was used to compare the means of each group. When multiple groups were compared at several time-points, a two-way ANOVA multiple comparison test was used. Tukey's method was used to correct for multiple comparisons. A P value of less than 0.05 was considered statistically significant. Figures show data as mean plus SEM.

RESULTS

Increased nonHDLc levels lead to loss of ambulatory function, reduction in stride length, and grossly observable hindlimb wasting in Dysf$^{-/-}$ApoE$^{-/-}$ mice

The experimental WT, ApoE$^{-/-}$, Dysf$^{-/-}$, and Dysf$^{-/-}$ApoE$^{-/-}$ mice showed no obvious ambulatory defect at birth. Being the most common model of rodent hyperlipidemia, the expected increase in plasma nonHDLc associated with ApoE gene inactivation and Western diet supplementation was confirmed by increases in total cholesterol and decreases in HDLc that were not statistically different between ApoE$^{-/-}$ and Dysf$^{-/-}$ApoE$^{-/-}$ groups (supplemental Fig. S1A, B). Although plasma TG levels were raised in Western diet-fed ApoE$^{-/-}$ vs. WT mice, there was no statistically significant difference between Dysf$^{-/-}$ApoE$^{-/-}$ and Dysf$^{-/-}$ groups (supplemental Fig. S1C). Chow-fed ApoE$^{-/-}$ and Dysf$^{-/-}$ApoE$^{-/-}$ animals had total cholesterol levels greater than WT and Dysf$^{-/-}$ mice but significantly lower than ApoE$^{-/-}$ and Dysf$^{-/-}$ApoE$^{-/-}$ groups fed a Western diet (supplemental Fig. S1A).

At 11 mo, 40% of Dysf$^{-/-}$ApoE$^{-/-}$ animals on a Western diet showed severe ambulation dysfunction, manifested as complete loss of hindlimb mobility whereas forelimbs remained functional albeit visibly weakened (**Fig.1A**), while WT, ApoE$^{-/-}$, and Dysf$^{-/-}$ mice on a Western diet as well as Dysf$^{-/-}$ApoE$^{-/-}$ on a chow diet showed no signs of ambulatory dysfunction by 11 mo (Fig. 1B). A decline in stride length relative to controls was observed exclusively in Dysf$^{-/-}$ApoE$^{-/-}$ mice on a Western diet and occurred suddenly around the 11 mo time-point (Fig. 1C); however, this effect was not observed in Western diet-fed animals at 4 or 7 mo time-points or in chow-fed Dysf$^{-/-}$ApoE$^{-/-}$ mice (Fig. 1D). Following euthanasia, a significant reduction in lower hindlimb width was noted between Western diet-fed Dysf$^{-/-}$ApoE$^{-/-}$ mice and WT, ApoE, and Dysf$^{-/-}$ groups at 11 mo of age without significant difference at 7 mo of age (**Fig. 2A**, B). Interestingly, chow-fed Dysf$^{-/-}$ApoE$^{-/-}$ mice did not display any reduction in hindlimb size observed in Western diet-fed animals at 11 mo (Fig. 2A). This suggests that the drastic elevation in nonHDLc in Dysf$^{-/-}$ApoE$^{-/-}$ mice caused by the combination of ApoE-deficiency and a Western diet can significantly exacerbate the mild dysferlinopathy phenotype in the murine model and lead to complete loss of ambulation.

Increased nonHDLc levels do not affect muscle pathology ex vivo muscle function in Dysf$^{-/-}$ diaphragm and soleus muscles

Because Dysf$^{-/-}$ApoE$^{-/-}$ mice exhibit severe ambulation dysfunction, we investigated the contractile properties of their muscles via muscle strip and whole muscle ex vivo myography. This was done at the 11 mo time-point for all Western diet-fed groups using diaphragm strips and whole soleus muscles because of their ease of isolation and mounting. To our surprise, no changes were observed in soleus or diaphragm muscle fatigue and postfatigue force recovery, except Dysf$^{-/-}$ApoE$^{-/-}$ diaphragm muscles were found to maintain muscle force after repeated stimulation better than other groups at 11 mo (Fig. 2C, D). As the assessment of ex vivo muscle function parameters in the soleus and diaphragm did not correlate to the dramatic impairment of ambulatory function observed, muscle morphology was analyzed by histology. Histological sections revealed no overt pathology in the soleus or diaphragm muscles (**Fig. 3A**, E) and quantification of soleus muscle size and composition showed no evidence of muscle wasting or remodelling on a Western diet by 11 mo (Fig. 3B–D). This suggests that impairment of ambulatory function observed in Dysf$^{-/-}$ApoE$^{-/-}$ mice is likely not due to primary impairment of muscle force and function when stimulated ex vivo.

Dysf$^{-/-}$ApoE$^{-/-}$ mice show severe exacerbation of muscle wasting, fatty infiltration, and inflammation in limb and girdle muscles without affecting fibrosis or percentage CNF

Masson's trichrome staining revealed normal muscle morphology in all WT and ApoE$^{-/-}$ muscles examined. As expected, minor wasting was detected in the rectus femoris (rec. fem.) segment of the quadriceps femoris muscle in Dysf$^{-/-}$ mice, while severe exacerbation of Dysf$^{-/-}$ damage and typical fibrofatty infiltration was detected in Dysf$^{-/-}$ApoE$^{-/-}$ rec. fem., both on chow and Western diets (**Fig. 4A**, B). Quantification revealed significant but similar reduction in cross-sectional area of rec. fem. at 11 mo of age in Dysf$^{-/-}$ApoE$^{-/-}$ and Dysf$^{-/-}$ mice compared with WT and ApoE controls both on chow and Western diets (Fig.4C). However, analysis of rec. fem. muscle composition

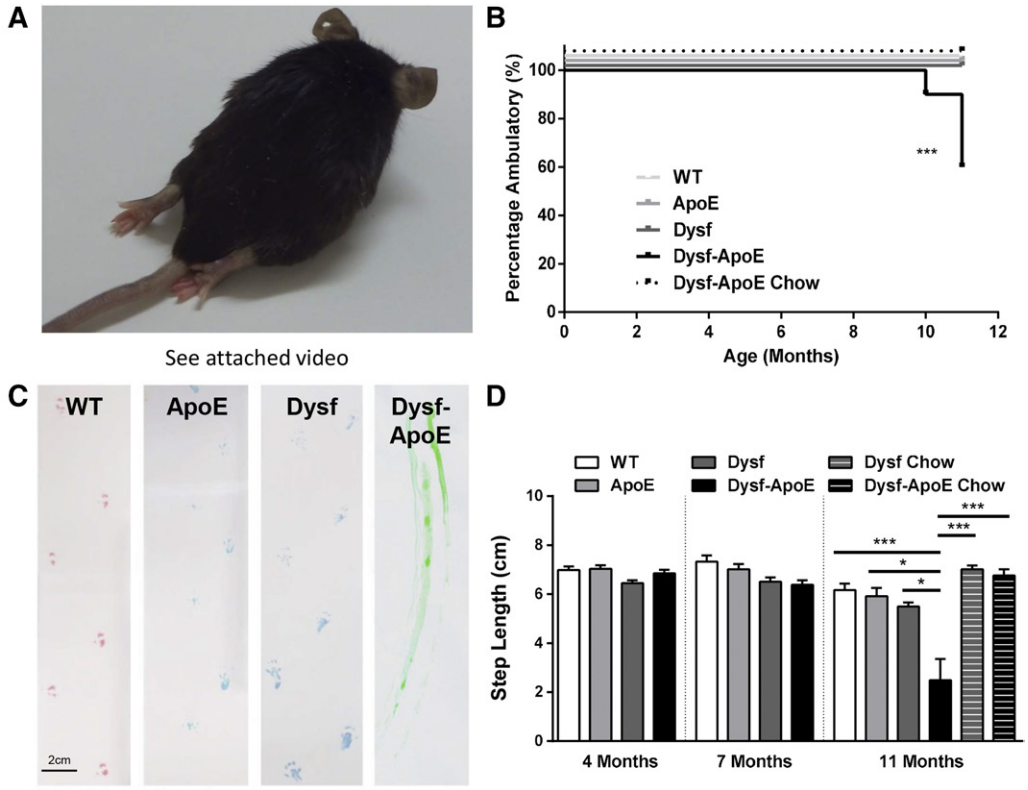

Fig. 1. ApoE-deficiency causes loss of ambulatory function and reduced step length in Dysf$^{-/-}$ mice. Image/video of an unanesthetized and unrestricted 10-month-old Dysf$^{-/-}$ApoE$^{-/-}$ mouse on Western diet with severe ambulation dysfunction, showing complete lost hindlimb function with residual forelimb function (A). Longitudinal observation of mice reveals a loss of ambulatory function in 40% of Dysf$^{-/-}$ApoE$^{-/-}$ mice on a Western diet by 11 mo, compared with 0% in all other Western diet-fed groups and Dysf$^{-/-}$ApoE$^{-/-}$ mice on a chow diet (B). Based on gait measurements, such as these representative traces of 11-month-old mice on a Western diet (C), there was a significant reduction in the step length of Dysf$^{-/-}$ApoE$^{-/-}$ mice at 11 months of age on a Western diet compared with all other groups on a Western diet and Dysf$^{-/-}$ApoE$^{-/-}$ mice on a chow diet (D). Mean + SEM. *$P < 0.05$; ***$P < 0.001$.

revealed a drastic increase in fatty replacement (Fig. 4D) and a reduction in healthy myofiber content (Fig. 4E) within the muscle in Dysf$^{-/-}$ApoE$^{-/-}$ compared with all other groups of mice on chow at 11 mo, and this effect was further exacerbated with Western diet supplementation. In the most severe cases, 11 mo Dysf$^{-/-}$ApoE$^{-/-}$ mice fed a Western diet displayed hindlimb width reduced to less than 4 mm with fatty infiltration of the rec. fem. reaching up to 91% of the total muscle area (supplemental Fig. S1D). Interestingly, loss of ApoE did not affect the percentage of fibrosis in Dysf$^{-/-}$ mice at 11 mo on either chow or Western diet (Fig. 4F).

Muscle wasting was not exclusive to rec. fem., as analysis of triceps brachii muscle of chow-fed animals revealed a similar pattern of pathology seen in the rec. fem. (**Fig. 5A**) with a drastic muscle remodelling in Dysf$^{-/-}$ApoE$^{-/-}$ mice in comparison to Dysf$^{-/-}$ mice, which was significantly exacerbated by Western diet supplementation (Fig. 5B). Although triceps brachii muscle wasting and fibrosis were similar between Dysf$^{-/-}$ and Dysf$^{-/-}$ApoE$^{-/-}$ mice (Fig. 5C), Dysf$^{-/-}$ApoE$^{-/-}$ mice exhibited increased fatty infiltration as well as significant reduction in healthy myofiber area on chow and Western diets (Fig. 5D–F). In addition, gastrocnemius muscle was associated with damage at 11 mo on Western diet (supplemental Fig. S2A), displaying minor, nonsignificant damage in Dysf$^{-/-}$ tissue while Dysf$^{-/-}$ApoE$^{-/-}$ mice exhibited significant fatty infiltration and loss of viable muscle area (supplemental Fig. S2B–D). Tibialis anterior muscles showed a similar but even less severe pattern of pathology (supplemental Fig. S3A), with Dysf$^{-/-}$ApoE$^{-/-}$ mice exhibiting a significant increase in fatty replacement and reduction in myofiber content compared with Dysf$^{-/-}$ mice with minor differences in cross-sectional area at 11 months of age on a Western diet (supplemental Fig. S3B–D).

High incidence of skeletal muscle and vascular abnormalities in Dysf$^{-/-}$ApoE$^{-/-}$ muscles

Rec. fem. and triceps brachii muscle analyses by a board-certified pathologist revealed vascular extravasation of inflammatory cell accumulation in muscle tissue (**Fig.6A**), which was found to be significantly increased in Dysf$^{-/-}$ApoE$^{-/-}$ triceps brachii compared with all other groups (Fig. 6G). Moreover, we detected the presence of cholesterol pits in and around every (100%) Western diet-fed Dysf$^{-/-}$ApoE$^{-/-}$ rec. fem. muscle, whereas cholesterol pitting was not detected in any (0%) tissues from other

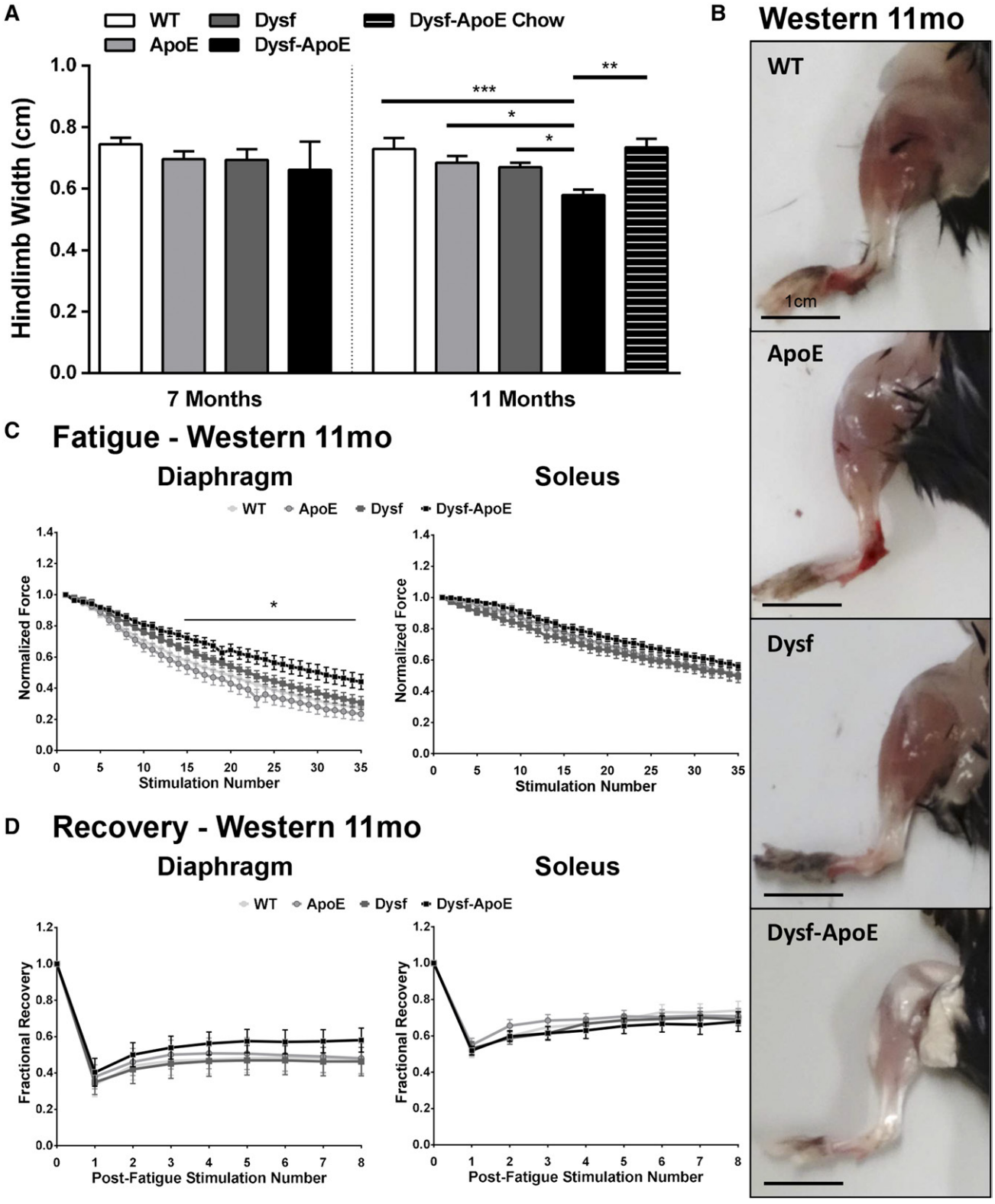

Fig. 2. Dysf$^{-/-}$ApoE$^{-/-}$ mice display gross hindlimb atrophy without significant effect on ex vivo muscle function. Hindlimb size is reduced in Western diet-fed Dysf$^{-/-}$ApoE$^{-/-}$ mice compared with all other Western diet-fed groups at 11 mo as well as Dysf$^{-/-}$ApoE$^{-/-}$ 11-month-old mice on a chow diet (A), as seen in representative skinned legs of 11-month-old Western diet-fed mice (B). By 11 months of age on a Western diet, a minor improvement of diaphragm muscle force maintenance was observed during fatigue of Dysf$^{-/-}$ApoE$^{-/-}$ diaphragm muscles but no dramatic changes in soleus muscle fatigue (C). Force recovery in the diaphragm and soleus force recovery were similarly unaffected by 11 months of age on a Western diet (D). Mean ± SEM. *$P < 0.05$; **$P < 0.01$; ***$P < 0.001$.

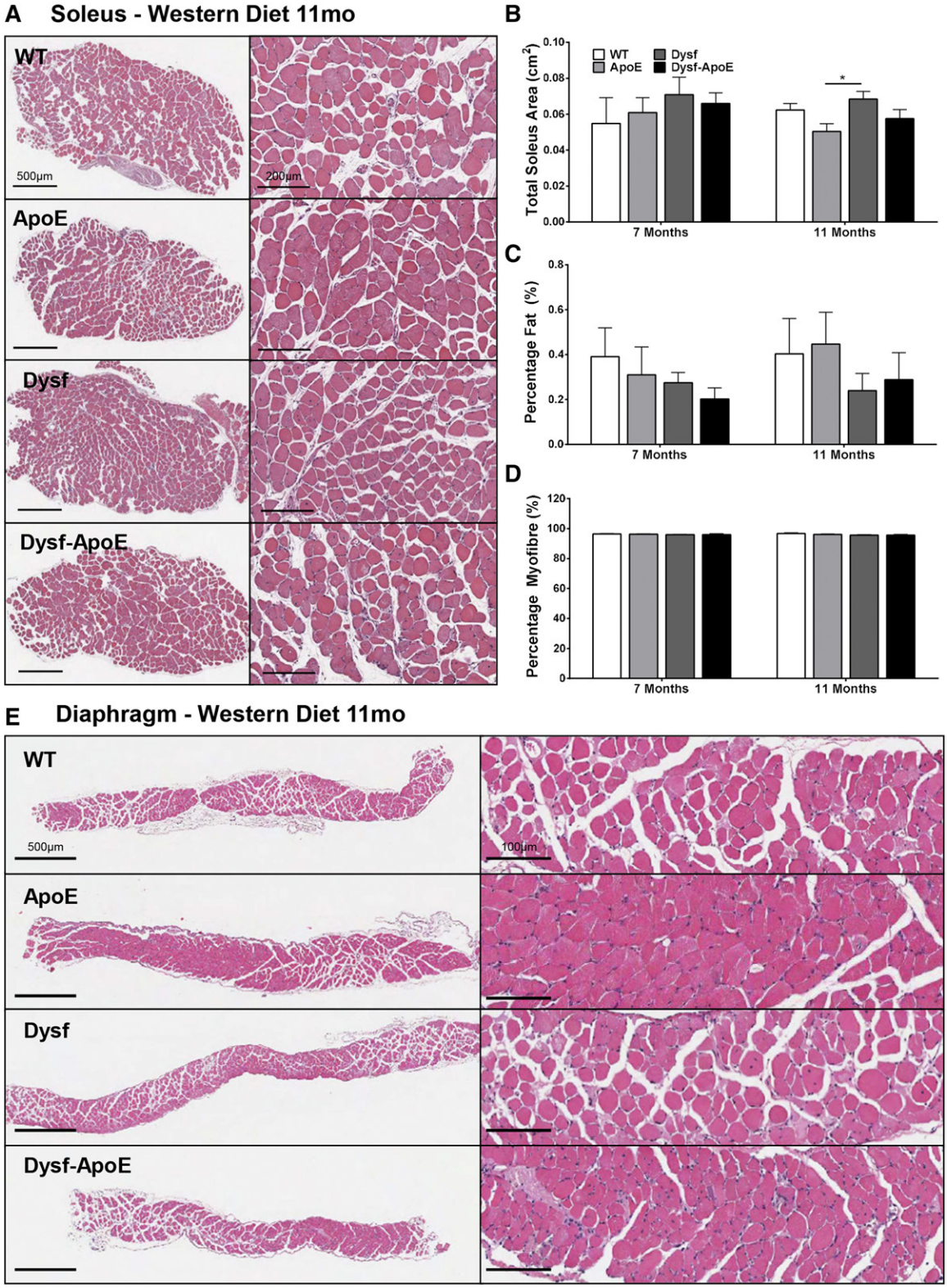

Fig. 3. Histological analysis of soleus and diaphragm muscles. Representative images of H&E stained soleus (A) and diaphragm (E) muscles from Western diet-fed groups at 11 mo. Quantification of soleus total area (B), percentage of fat content (C), and percentage of myofiber content (D), displaying no evidence of significant muscle pathology in any group. Mean + SEM. $*P < 0.05$.

groups (Fig. 6B, H). Interestingly, areas of muscle calcification were observed in both Dysf$^{-/-}$ and Dysf$^{-/-}$ApoE$^{-/-}$ muscle (Fig. 6C) at 7 mo of age, which by 11 mo of age was mainly replaced by fibrofatty infiltration and cholesterol. In regions of dramatic remodelling, the presence of significant adipocyte replacement was confirmed via immunofluorescence staining for perilipin-1, an adipocyte marker, in Dysf$^{-/-}$ApoE$^{-/-}$ triceps brachii muscle, which can be

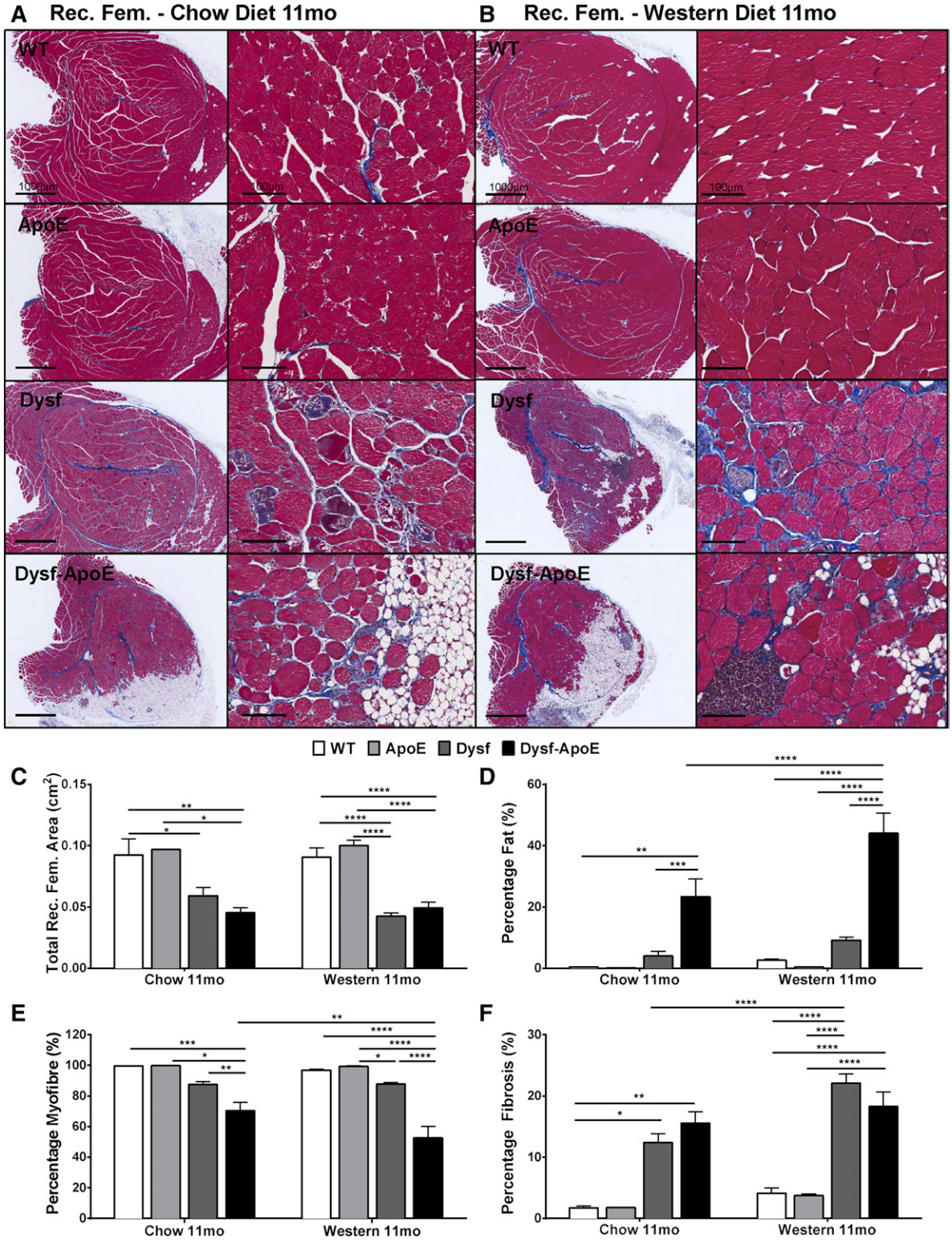

Fig. 4. Histological analysis of rec. fem. muscle. Representative images of Masson's trichrome staining of rec. fem. muscles from 11-month-old WT, ApoE$^{-/-}$, Dysf$^{-/-}$, and Dysf$^{-/-}$ApoE$^{-/-}$ groups fed chow (A) or Western diets (B) with comparison of total rec. fem. area (C), percentage of fat content (D), percentage of myofiber content (E), and percentage of fibrosis (F), demonstrating a highly significant shift in muscle size and composition of chow- and Western diet-fed Dysf$^{-/-}$ApoE$^{-/-}$ animals at 11 mo. Mean + SEM. *P< 0.05; **P< 0.01; ***P< 0.001; ****P< 0.0001.

seen in red, counterstained with nuclear stain DAPI in blue (Fig. 6D). In order to further characterize the lipid accumulation in these muscles, Oil Red O stained sections of 11-month-old Western diet-fed groups showed significant neutral lipid deposition in large areas within Dysf$^{-/-}$ApoE$^{-/-}$ triceps brachii muscle with little fat infiltration observed

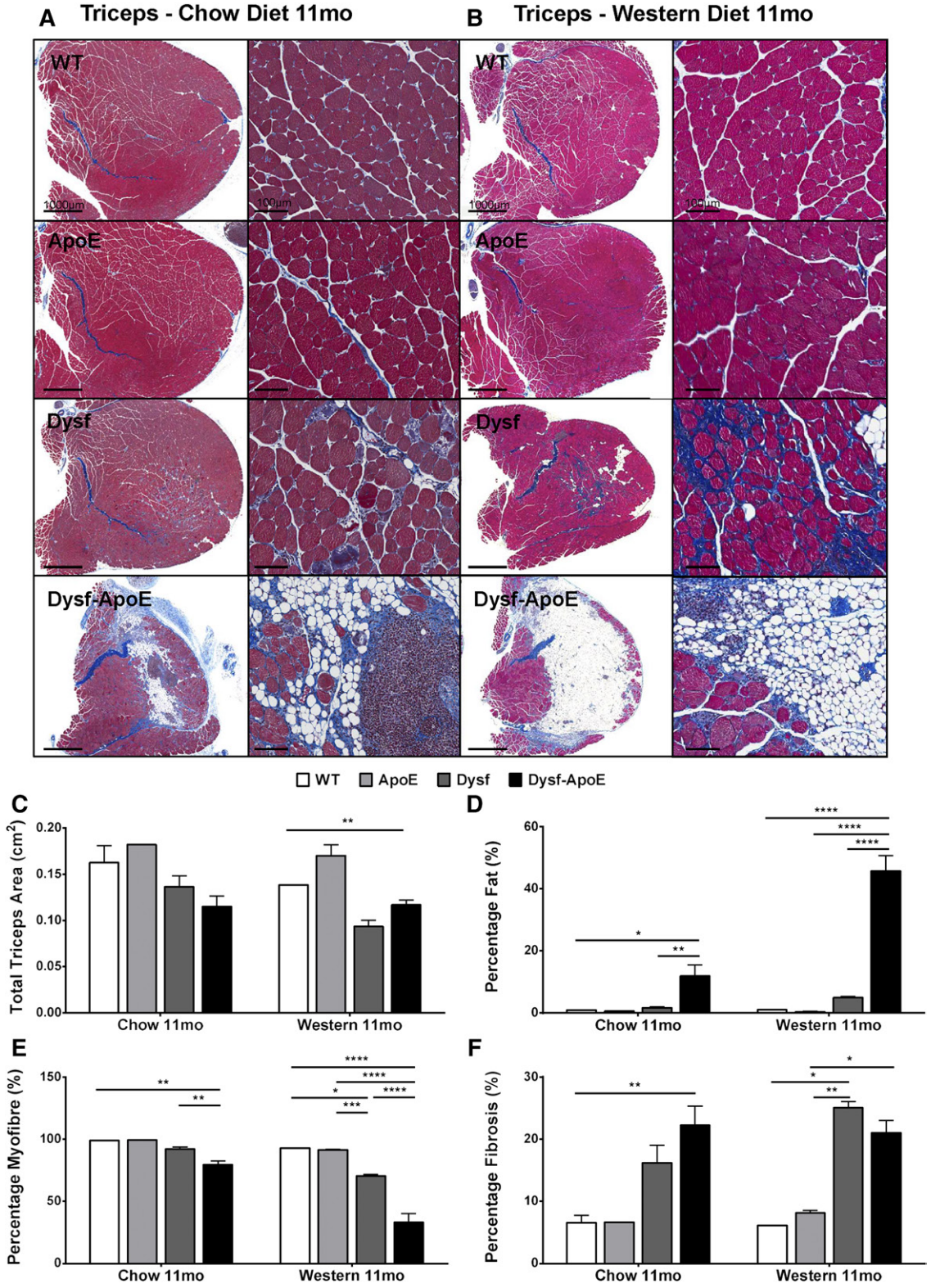

Fig. 5. Histological analysis of triceps brachii muscle. Representative images of Masson's trichrome staining of triceps brachii muscles from 11-month-old WT, ApoE$^{-/-}$, Dysf$^{-/-}$ and Dysf$^{-/-}$ApoE$^{-/-}$ groups fed chow (A) or Western diets (B) with comparison of total triceps brachii area (C), percentage of fat content (D), percentage of myofiber content (E), and percentage of fibrosis (F), demonstrating dramatically worsened muscle pathology by 11 mo in Dysf$^{-/-}$ApoE$^{-/-}$ animals on a Western diet compared with chow-fed animals. Mean + SEM. *P < 0.05; **P < 0.01; ***P < 0.001; ****P < 0.0001.

in Dysf$^{-/-}$ muscle (Fig. 6E, F). Despite the significant increase in muscle damage in Dysf$^{-/-}$ApoE$^{-/-}$ compared with Dysf$^{-/-}$ mice, the percentage of CNF was not significantly different between Dysf-deficient groups in the rec. fem. (Fig. 6I) and triceps brachii (Fig. 6J) at 11 months of age on a Western diet.

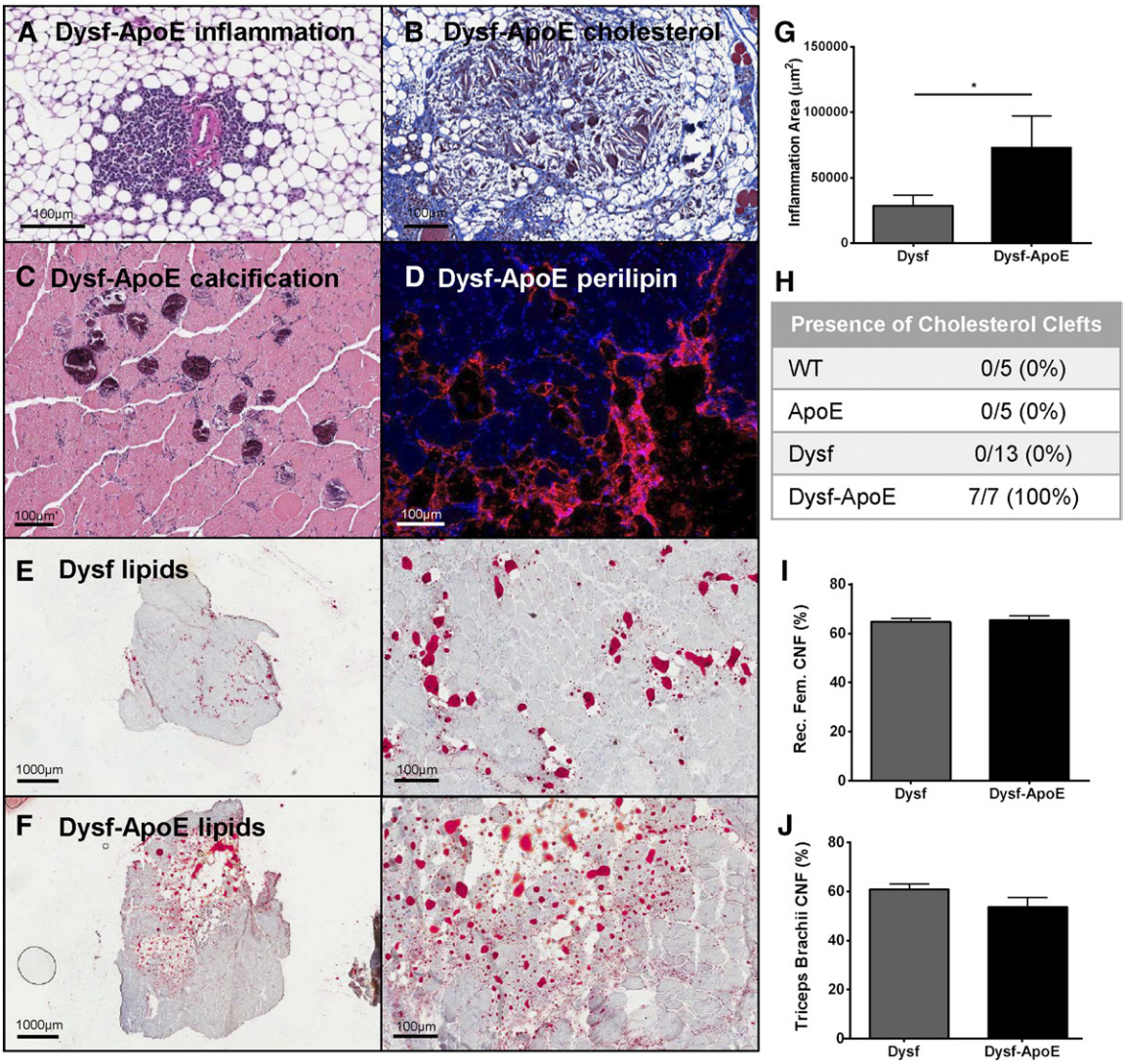

Fig. 6. Vascular and muscle abnormalities observed in Dysf$^{-/-}$ApoE$^{-/-}$ mice without affecting percentage CNF. Perivascular infiltration of inflammatory cells was only observed in Dysf$^{-/-}$ApoE$^{-/-}$ muscles (A) as well as deposition of cholesterol clefts (B) and calcification (C). Confirmation of adipocyte presence in muscles via perilipin-1 stain (red) was found in areas of Dysf$^{-/-}$ApoE$^{-/-}$ muscle damage, nuclei stained with DAPI (blue) (D), and by Oil Red O staining of triceps brachii muscles (neutral lipids in red) (E, F). Quantification of inflammatory cell area revealed increased infiltration in Dysf$^{-/-}$ApoE$^{-/-}$ muscle (G) and presence of cholesterol clefts was observed in 100% of Dysf$^{-/-}$ApoE$^{-/-}$ muscles (H). No differences were observed in the percentage CNFs between Dysf$^{-/-}$ and Dysf$^{-/-}$ApoE$^{-/-}$ groups in the rec. fem. (I) or triceps brachii (J) muscles. Mean + SEM. *$P < 0.05$.

ApoE-deficiency in Dysf$^{-/-}$ mice has no effect on cardiac muscle pathology

Although cardiac dysfunction is not always observed in dysferlinopathic patients, Dysf expression was reported in cardiomyocytes and some studies have shown minor changes in the cardiac function parameters of Dysf-deficient mice by echocardiogram (18). However, in vivo functional analysis showed no significant differences in cardiac function or in ventricular wall thickness (supplemental Fig. S4) and thus supports the overall conclusion that although Dysf$^{-/-}$ApoE$^{-/-}$ mice show signs of significant vascular abnormalities, no cardiac pathology was observed.

DISCUSSION

The data presented herein support the conclusion that ApoE gene inactivation in combination with a Western diet, which lead to increased cholesterol, can severely exacerbate skeletal muscle pathology in the Dysf$^{-/-}$ model of LGMD2B. The single Dysf$^{-/-}$ model is known to exhibit mild muscle pathology compared with dysferlinopathic patients (19), whereas the Dysf$^{-/-}$ApoE$^{-/-}$ mice described herein display severe muscle wasting and remodeling as well as the complete loss of ambulatory function in nearly half of the mice fed a Western diet. Hence, we propose that this model more closely recapitulates human manifestations of LGMD2B. Although very old Dysf-deficient mice display significant lipid accumulation in some muscles (20, 21), the level of fat infiltration by 11 mo in our Dysf$^{-/-}$ApoE$^{-/-}$ muscles is even more severe and more representative of human disease, leading to dramatic locomotor dysfunction, which is a definitive end-point of LGMD2B patients. This occurred with a high degree of selectivity, as ApoE inactivation did not affect muscle integrity

in nonlimb/girdle muscles. Indeed, dysferlinopathic patients typically exhibit fibrofatty replacement in classic limb-girdle muscles, including rec. fem. and triceps brachii with occasionally gastrocnemius and tibialis anterior muscles, whereas vital respiratory and cardiac muscles are generally spared (2). In our $Dysf^{-/-}ApoE^{-/-}$ mice, a similar pattern of muscle damage was observed, leaving diaphragm and soleus muscles along with cardiac function unaffected by ApoE-deficiency.

In addition, a previous study from our group found that elevated nonHDLc in Duchenne MD also led to worsened *mdx* mouse muscle pathology but with a distinct affected muscle pattern and phenotype: more fibrosis than fatty infiltration occurring at earlier time-points and affecting triceps brachii, gastrocnemius, and diaphragm muscles more severely while sparing rec. fem (22). This suggests that the effects of nonHDLc on muscle integrity are complex and not simply through generalized muscle ischemia or severe muscle perfusion abnormalities, as elevated nonHDLc exacerbates muscle pathology differently based on the type of MD investigated. It is important to note that an increase in nonHDLc levels in our $Dysf^{-/-}ApoE^{-/-}$ model did not change the established pattern of muscles affected by loss of Dysf but rather accelerated primary disease progression. The reason why only limb and girdle-area muscles are effected in dysferlinopathies is not well understood; differences in muscle fiber types (23) has been proposed, whereas our data suggest that the possibility of vascular bed heterogeneities between different muscles, such as those arising from organ-specific endothelial differentiation, warrant further investigation.

While skeletal muscle-specific overexpression of Dysf has been shown to rescue the mild MD phenotype of Dysf-deficient animals (8), we and others have reported positive Dysf expression in nonmuscle cells, such as vascular smooth muscle and endothelial cells as well as inflammatory cells, and that loss of Dysf expression causes vascular abnormalities (3, 24). We believe that the role that these vascular abnormalities play in the development of muscle pathology was stressed by generating $Dysf^{-/-}$ animals with plasma lipid profiles associated with vascular disease. The drastic exacerbation of muscle wasting we observed combined with indices of vascular permeability and increased inflammation shed a new light on the 'vascular hypothesis' in MD (11). Generally dismissed as a major player in MD due to the lack of micro-infarcts in MD muscle tissues, vascular abnormalities can nonetheless be seen in preclinical biopsies and animal models of other types of MD before muscle damage (10, 22). In our model, the significant areas of inflammatory cell and adipocyte aggregation around large blood vessels suggest that the endothelial barrier is compromised and that the effectors of muscle damage and remodeling could be of vascular origin. Combined with a report that Dysf expression is modulated in leaky and inflamed vessels (25), our data support the concept that disruption of vascular barrier function in $Dysf^{-/-}$ muscles results in chronic leakage of plasma lipids into muscle tissue, thus exacerbating the primary $Dysf^{-/-}$ muscle defect through an unknown mechanism.

How heightened levels of nonHDLc exacerbate $Dysf^{-/-}$ myofiber damage, whether through direct myofiber toxicity or through changes in the muscle environment/signaling, remains to be investigated. Our data show a striking correlation between muscle disease severity and nonHDLc levels; for instance, $Dysf^{-/-}ApoE^{-/-}$ mice on a chow diet exhibited intermediate nonHDLc levels and muscle pathology between $Dysf^{-/-}$ and $Dysf^{-/-}ApoE^{-/-}$ groups on a Western diet. In contrast, no significant relationship to TG levels was observed, suggesting that nonHDLc plays the major role in muscle pathology exacerbation in our model. Because Dysf is known to interact with anionic phospholipids and facilitate sarcolemma repair, it is possible that cholesterol- and lipid-rich environments may have unexpected effects on blunted sarcolemmal repair processes found in Dysf-deficient myofibers (26–29). Cholesterol has been shown to be a key player in exocytosis and vesicle trafficking, where addition or depletion of cholesterol from the plasma membrane lead to dysregulated Ca^{2+}-triggered vesicle fusion (27). One study showed that depletion of cholesterol led to improved myoblast fusion and that cholesterol may also play a role in early myofiber differentiation (29). Another potential effect of increased nonHDLc infiltration of muscle tissue is through a change in oxidative stress in the muscle environment. Previous studies have shown that oxidative stress is increased in Dysf-deficient muscle and in other forms of MD, and that this elevation in reactive oxygen species correlates with muscle damage (30–33). Therefore, as reactive oxygen species are known to be increased in the context of hyperlipidemia and vascular disease (34), heightened oxidative stress and free radical-mediated injury may have a significant effect on muscle integrity. On the other hand, destruction of Dysf-deficient myofibers may also be mediated by recruited inflammatory cells, found in great abundance in $Dysf^{-/-}ApoE^{-/-}$ muscle. Increased immune cell reactivity could result in direct death of susceptible Dysf-deficient myofiber but may also affect muscle remodelling through the release of signaling molecules, triggering fibrofatty replacement of damaged areas instead of promoting myofiber regeneration.

Although our model of dysferlinopathy shows greater similarities to human pathology than other murine models of the disease, there are some important caveats to consider. First, caution must be taken when comparing the lipid profiles of $ApoE^{-/-}$ mice and dysferlinopathic patients. Lipid abnormalities have been observed in LGMD2B patients (12), however loss of ApoE causes a moderate elevation in LDL and IDL along with a dramatic increase in chylomicrons and VLDL to levels rarely seen in humans (35). Moreover, although ApoE is predominantly expressed in the liver for reverse cholesterol transport, it also expressed in peripheral tissues such as adipose tissue and macrophages (36, 37), which may affect whole body lipid metabolism and inflammatory responses. Another important consideration is that contrary to studies that found significant impairment of locomotor function (38, 39) and muscle function ex vivo (40) in other LGMD2B mouse models, we did not observe

any significant reduction in step length or muscle function in Dysf$^{-/-}$ mice. This is likely due to the disparity between Dysf-deficient strains (A/J, Bla/J, or SJL) and the Dysf-null (Dysf$^{-/-}$) model used in this study, all of which have different levels of Dysf expression in the muscle and exhibit some important phenotypic differences (19, 41). However, it should be noted that our ex vivo muscle function data correlate with a lack of damage or remodelling in the soleus and diaphragm, whereas other groups found significant areas of fibrosis and damage in muscles that exhibited impaired function ex vivo (38, 40), further highlighting the differences between the various models of dysferlinopathies.

The authors wish to thank Prof. Miranda Grounds for her technical assistance, advice, and guidance during the writing of this manuscript.

REFERENCES

1. Bansal, D., K. Miyake, S. S. Vogel, S. Groh, C. C. Chen, R. Williamson, P. L. McNeil, and K. P. Campbell. 2003. Defective membrane repair in dysferlin-deficient muscular dystrophy. *Nature.* **423:** 168–172.
2. Urtizberea, J. A., G. Bassez, F. Leturcq, K. Nguyen, M. Krahn, and N. Levy. 2008. Dysferlinopathies. *Neurol. India.* **56:** 289–297.
3. Sharma, A., C. Yu, C. Leung, A. Trane, M. Lau, S. Utokaparch, F. Shaheen, N. Sheibani, and P. Bernatchez. 2010. A new role for the muscle repair protein dysferlin in endothelial cell adhesion and angiogenesis. *Arterioscler. Thromb. Vasc. Biol.* **30:** 2196–2204.
4. Han, R., D. Bansal, K. Miyake, V. P. Muniz, R. M. Weiss, P. L. McNeil, and K. P. Campbell. 2007. Dysferlin-mediated membrane repair protects the heart from stress-induced left ventricular injury. *J. Clin. Invest.* **117:** 1805–1813.
5. Cai, C., N. Weisleder, J. K. Ko, S. Komazaki, Y. Sunada, M. Nishi, H. Takeshima, and J. Ma. 2009. Membrane repair defects in muscular dystrophy are linked to altered interaction between MG53, caveolin-3, and dysferlin. *J. Biol. Chem.* **284:** 15894–15902.
6. Cenacchi, G., M. Fanin, L. B. De Giorgi, and C. Angelini. 2005. Ultrastructural changes in dysferlinopathy support defective membrane repair mechanism. *J. Clin. Pathol.* **58:** 190–195.
7. Han, R., E. P. Rader, J. R. Levy, D. Bansal, and K. P. Campbell. 2011. Dystrophin deficiency exacerbates skeletal muscle pathology in dysferlin-null mice. *Skelet. Muscle.* **1:** 35.
8. Millay, D. P., M. Maillet, J. A. Roche, M. A. Sargent, E. M. McNally, R. J. Bloch, and J. D. Molkentin. 2009. Genetic manipulation of dysferlin expression in skeletal muscle: novel insights into muscular dystrophy. *Am. J. Pathol.* **175:** 1817–1823.
9. Kesari, A., M. Fukuda, S. Knoblach, R. Bashir, G. A. Nader, D. Rao, K. Nagaraju, and E. P. Hoffman. 2008. Dysferlin deficiency shows compensatory induction of Rab27A/Slp2a that may contribute to inflammatory onset. *Am. J. Pathol.* **173:** 1476–1487.
10. Miike, T., S. Sugino, Y. Ohtani, K. Taku, and K. Yoshioka. 1987. Vascular endothelial cell injury and platelet embolism in Duchenne muscular dystrophy at the preclinical stage. *J. Neurol. Sci.* **82:** 67–80.
11. Lombard, J. H. 2011. Microcirculation in a mouse model of Duchenne muscular dystrophy: another blow to the vascular hypothesis? *J. Appl. Physiol. (1985)* **110:** 587–588.
12. Srivastava, N. K., R. Yadav, S. Mukherjee, L. Pal, and N. Sinha. 2017. Abnormal lipid metabolism in skeletal muscle tissue of patients with muscular dystrophy: In vitro, high-resolution NMR spectroscopy based observation in early phase of the disease. *Magn. Reson. Imaging.* **38:** 163–173.
13. Hughes, B. P. 1972. Lipid changes in Duchenne muscular dystrophy. *J. Neurol. Neurosurg. Psychiatry.* **35:** 658–663.
14. Temin, P. A., and I. B. Islamova. 1983. [Plasma lipids of patients with Duchenne's muscular dystrophy at different stages of the disease] *Zh. Nevropatol. Psikhiatr. Im. S. S. Korsakova.* **83:** 1632–1636. Russian.
15. Srivastava, N. K., S. Pradhan, B. Mittal, and G. A. Gowda. 2010. High resolution NMR based analysis of serum lipids in Duchenne muscular dystrophy patients and its possible diagnostic significance. *NMR Biomed.* **23:** 13–22.
16. Sharma, A., S. Sellers, N. Stefanovic, C. Leung, S. M. Tan, O. Huet, D. J. Granville, M. E. Cooper, J. B. de Haan, and P. Bernatchez. 2015. Direct eNOS activation provides atheroprotection in diabetes-accelerated atherosclerosis. *Diabetes.* **64:** 3937–3950.
17. Mehlem, A., C. E. Hagberg, L. Muhl, U. Eriksson, and A. Falkevall. 2013. Imaging of neutral lipids by oil red O for analyzing the metabolic status in health and disease. *Nat. Protoc.* **8:** 1149–1154.
18. Chase, T. H., G. A. Cox, L. Burzenski, O. Foreman, and L. D. Shultz. 2009. Dysferlin deficiency and the development of cardiomyopathy in a mouse model of limb-girdle muscular dystrophy 2B. *Am. J. Pathol.* **175:** 2299–2308.
19. Kobayashi, K., T. Izawa, M. Kuwamura, and J. Yamate. 2012. Dysferlin and animal models for dysferlinopathy. *J. Toxicol. Pathol.* **25:** 135–147.
20. Grounds, M. D., J. R. Terrill, H. G. Radley-Crabb, T. Robertson, J. Papadimitriou, S. Spuler, and T. Shavlakadze. 2014. Lipid accumulation in dysferlin-deficient muscles. *Am. J. Pathol.* **184:** 1668–1676.
21. Demonbreun, A. R., A. E. Rossi, M. G. Alvarez, K. E. Swanson, H. K. Deveaux, J. U. Earley, M. Hadhazy, R. Vohra, G. A. Walter, P. Pytel, et al. 2014. Dysferlin and myoferlin regulate transverse tubule formation and glycerol sensitivity. *Am. J. Pathol.* **184:** 248–259.
22. Milad, N., Z. White, A. Y. Tehrani, S. Sellers, F. M. V. Rossi, and P. Bernatchez. 2017. Increased plasma lipid levels exacerbate muscle pathology in the mdx mouse model of Duchenne muscular dystrophy. *Skelet. Muscle.* **7:** 19.
23. Glover, L. E., K. Newton, G. Krishnan, R. Bronson, R. Boyle, R. Krivickas, and R. H. J. Brown. 2010. Dysferlin overexpression in skeletal muscle produces a progressive myopathy. *Ann. Neurol.* **67:** 384–393.
24. Karsan, A., J. Blonder, J. Law, E. Yaquian, D. A. Lucas, T. P. Conrads, and T. Veenstra. 2005. Proteomic analysis of lipid microdomains from lipopolysaccharide-activated human endothelial cells. *J. Proteome Res.* **4:** 349–357.
25. Hochmeister, S., R. Grundtner, J. Bauer, B. Engelhardt, R. Lyck, G. Gordon, T. Korosec, A. Kutzelnigg, J. J. Berger, M. Bradl, et al. 2006. Dysferlin is a new marker for leaky brain blood vessels in multiple sclerosis. *J. Neuropathol. Exp. Neurol.* **65:** 855–865.
26. Ameziane-Le Hir, S., C. Raguenes-Nicol, G. Paboeuf, A. Nicolas, E. Le Rumeur, and V. Vie. 2014. Cholesterol favors the anchorage of human dystrophin repeats 16 to 21 in membrane at physiological surface pressure. *Biochim. Biophys. Acta.* 1838: 1266–1273.
27. Churchward, M. A., T. Rogasevskaia, J. Hofgen, J. Bau, and J. R. Coorssen. 2005. Cholesterol facilitates the native mechanism of Ca2+-triggered membrane fusion. *J. Cell Sci.* **118:** 4833–4848.
28. Logan, D. M., and K. H. Tsang. 1992. Cholesterol alterations in young dystrophic mice. *Mol. Cell. Biochem.* **110:** 55–64.
29. Mermelstein, C. S., D. M. Portilho, R. B. Medeiros, A. R. Matos, M. Einicker-Lamas, G. G. Tortelote, A. Vieyra, and M. L. Costa. 2005. Cholesterol depletion by methyl-beta-cyclodextrin enhances myoblast fusion and induces the formation of myotubes with disorganized nuclei. *Cell Tissue Res.* **319:** 289–297.
30. Rando, T. A., M-H. Disatnik, Y. Yu, and A. Franco. 1998. Muscle cells from *mdx* mice have an increased susceptibility to oxidative stress. *Neuromuscul. Disord.* **8:** 14–21.
31. Tidball, J. G., and M. Wehling-Henricks. 2007. The role of free radicals in the pathophysiology of muscular dystrophy. *J. Appl. Physiol. (1985)* **102:** 1677–1686.
32. Whitehead, N. P., E. W. Yeung, and D. G. Allen. 2006. Muscle damage in *mdx* (dystrophic) mice: role of calcium and reactive oxygen species. *Clin. Exp. Pharmacol. Physiol.* **33:** 657–662.
33. Terrill, J. R., H. G. Radley-Crabb, T. Iwasaki, F. A. Lemckert, P. G. Arthur, and M. D. Grounds. 2013. Oxidative stress and pathology in muscular dystrophies: focus on protein thiol oxidation and dysferlinopathies. *FEBS J.* **280:** 4149–4164.
34. Förstermann, U. 2010. Nitric oxide and oxidative stress in vascular disease. *Pflugers Arch.* **459:** 923–939.
35. Piedrahita, J. A., S. H. Zhang, J. R. Hagaman, P. M. Oliver, and N. Maeda. 1992. Generation of mice carrying a mutant apolipoprotein E gene inactivated by gene targeting in embryonic stem cells. *Proc. Natl. Acad. Sci. USA.* **89:** 4471–4475.

36. Tenger, C., X. Zhou. 2003. Apolipoprotein E modulates immune activation by acting on the antigen-presenting cell. Immunology. 109: 392–397.
37. Baitsch, D., H. H. Bock, T. Engel, R. Telgmann, C. Muller-Tidow, G. Varga, M. Bot, J. Herz, H. Robenek, A. von Eckardstein, et al. 2011. Apolipoprotein E induces antiinflammatory phenotype in macrophages. *Arterioscler. Thromb. Vasc. Biol.* **31:** 1160–1168.
38. Sondergaard, P. C., D. A. Griffin, E. R. Pozsgai, R. W. Johnson, W. E. Grose, K. N. Heller, K. M. Shontz, C. L. Montgomery, J. Liu, K. R. Clark, et al. 2015. AAV.Dysferlin overlap vectors restore function in dysferlinopathy animal models. *Ann. Clin. Transl. Neurol.* **2:** 256–270.
39. Nagy, N., R. J. Nonneman, T. Llanga, C. F. Dial, N. V. Riddick, T. Hampton, S. S. Moy, K. K. Lehtimaki, T. Ahtoniemi, J. Puolivali, et al. 2017. Hip region muscular dystrophy and emergence of motor deficits in dysferlin-deficient Bla/J mice. *Physiol. Rep.* **5:** 1–16.
40. Barton, E. R., B. J. Wang, B. K. Brisson, and H. L. Sweeney. 2010. Diaphragm displays early and progressive functional deficits in dysferlin-deficient mice. *Muscle Nerve.* **42:** 22–29.
41. Kobayashi, K., T. Izawa, M. Kuwamura, and J. Yamate. 2010. The distribution and characterization of skeletal muscle lesions in dysferlin-deficient SJL and A/J mice. *Exp. Toxicol. Pathol.* **62:** 509–517.